

# Diurnal variation and the influential factors of precipitation from surface and satellite measurements in Tibet

Jianping Guo,<sup>a,b</sup> Panmao Zhai,<sup>c\*</sup> Lu Wu,<sup>d</sup> Maureen Cribb,<sup>b</sup> Zhanqing Li,<sup>b</sup> Zhaoyan Ma,<sup>e</sup>  
Fu Wang,<sup>f</sup> Duo Chu,<sup>g</sup> Pengxiang Wang<sup>g</sup> and Jiahua Zhang<sup>h</sup>

<sup>a</sup> Institute of Atmospheric Composition, Chinese Academy of Meteorological Sciences, Beijing, China

<sup>b</sup> Department of Atmospheric and Oceanic Science & ESSIC, University of Maryland, College Park, MD, USA

<sup>c</sup> State Key Laboratory of Severe Weather, Chinese Academy of Meteorological Sciences, Beijing, China

<sup>d</sup> Henan Climate Center, Zhengzhou, China

<sup>e</sup> Shandong University of Science and Technology, Qingdao, China

<sup>f</sup> School of Resources and Environment, University of Electronic Science and Technology of China, Chengdu, China

<sup>g</sup> Tibet Institute of Plateau Atmospheric and Environmental Science Research, Tibet Meteorological Services, Lhasa, Tibet, China

<sup>h</sup> Center for Earth Observation and Digital Earth, Chinese Academy of Sciences, Beijing, China

**ABSTRACT:** Some new features concerning the diurnal variation of precipitation over the Tibetan Plateau (TP) are revealed from rainfall data acquired by a network of rain gauge stations and estimated by the Climate Precipitation Center Morphing (CMORPH) technique collected during the summer of 2010 and 2011. Maxima in precipitation amount and frequency are associated with the afternoon-to-evening precipitation regime at approximately 60% of the stations in the network. CMORPH data also capture this pattern, but miss the late morning peak that occurs at some stations. The timing of maximum occurrence agrees well with the diurnal cycle of synoptic conditions favouring the development of precipitation over this area. There is no distinct west-to-east propagation of the diurnal cycle, implying that the diurnal cycle is more driven by local effects than by large-scale circulation. It turns out that the diurnal cycle in precipitation frequency depends largely on topography and landscape. The geographical transition in precipitation peak time is distinct from hilly regions (daytime peak) towards lakes and valleys (evening-to-nocturnal peaks). Stations located in mountainous regions (valleys) tend to experience more precipitation in either late morning or early afternoon (late afternoon or evening). Overall, precipitation amount shows a similar topographic dependence, as does the precipitation frequency, suggesting that local-scale effects, such as the mountain valley circulation effect, has a great impact on the diurnal variation in precipitation when large-scale dynamical processes are weak. A possible mechanism for the non-uniform diurnal cycle of precipitation over the TP is proposed. The major conclusion is that plateau-scale synoptic systems, as well as local circulation systems caused by the complex topography, should be taken into account when determining the diurnal variation in precipitation over the TP.

**KEY WORDS** diurnal variation; precipitation; Tibetan Plateau; rain gauge; CMORPH

Received 5 July 2013; Revised 18 September 2013; Accepted 11 November 2013

## 1. Introduction

The Tibetan Plateau (TP) refers broadly to the region 4000 m above sea level (ASL) in western China, which also partly covers the territories of Bhutan, Nepal, India, Pakistan, and Afghanistan. The TP is the highest and largest plateau in the world. The surface elevation varies greatly across the plateau, particularly in the southernmost part, and strong contrasts in both land surface features (e.g. land cover type) and meteorological characteristics (moisture, temperature, precipitation, etc.) exist between western and eastern parts of the region (Ye and Gao, 1979). For some time, the TP has been receiving increasing attention because of its important

effects on weather and climate over Eurasia (Ding, 1994). The TP has a strong influence on the formation of the Asian monsoon (Yanai and Wu, 2006) because the uplifted plateau exerts direct dynamic and thermal forcings on the regional atmospheric circulation (Ye and Gao, 1979; Yanai *et al.*, 1992). The atmospheric circulation over the TP also has a distinct diurnal cycle in the summer (Krishnamurti and Kishtawal, 2000), which, along with local topographic and thermodynamic effects, likely complicates the diurnal variation in precipitation.

The diurnal cycle of precipitation has great implications not only for local weather, but also for local climate (Dai, 2001). In addition, the diurnal variation in precipitation is an important aspect of the hydrological cycle. From a modelling perspective, if these diurnal cycles can be captured objectively in numerical models, the warm-season rainfall predictability would be largely improved (Carbone and Tuttle, 2008).

\* Correspondence to: Panmao Zhai, Chinese Academy of Meteorological Sciences, 46, Zhongguancun South Avenue, Haidian District, Beijing 100081, China. E-mail: pmzhai@cma.gov.cn

Recent studies have investigated the diurnal variation in precipitation over the TP from ground-based measurements alone (Liu *et al.*, 2002; Yu *et al.*, 2007b). It was found that precipitation occurs most frequently during the late afternoon to evening over the northern part of the TP, which is largely attributed to existent thermodynamic conditions. Precipitation characteristics over the more complex terrain of the TP are yet to be determined due to the sparseness of stations collecting precipitation measurements. The merits of using satellite measurements, which can be collected over large areas, have prompted a proliferation of studies about the diurnal cycle of precipitation in this region (Sorooshian *et al.*, 2002; Wang *et al.*, 2005; Bai *et al.*, 2008; Yin *et al.*, 2008; Liu *et al.*, 2009; Singh and Nakamura, 2009).

On the basis of the Tropical Rainfall Measurement Mission (TRMM) precipitation radar (PR) data, both convective precipitation in the daytime (particularly in the afternoon) and stratiform precipitation in the evening and at night were thought to be the main precipitation types generating much of the rainfall in the northern part of the TP (Shimizu *et al.*, 2001). The diurnal variation of summertime precipitation over the eastern part of Tibet has been characterized using hourly infrared (IR) brightness temperatures derived from the Geostationary Meteorological Satellite (GMS; Wang *et al.*, 2005). Also, GMS/IR satellite data have been used to detect relative precipitation differences, such as contrasts in rainfall characteristics between the western and eastern parts of the TP (Ueno, 1998).

Although remote sensing from satellites generates precipitation information with a better spatial coverage compared to *in situ* ground-based measurements, the accurate retrieval of precipitation characteristics from space still faces many challenges. For example, the low Earth-orbiting TRMM PR, which has a high spatial resolution, cannot obtain measurements down to the Earth's surface over mountainous terrain (Houze, 2012). IR instruments onboard geostationary satellites have a relatively coarse spatial resolution, so cirrus or cold non-precipitating clouds can be easily mistaken for precipitation if IR data alone are used (Joyce *et al.*, 2004). The inconsistency between rain gauge-derived and TRMM microwave (MW)-retrieved rainfall has drawn attention to the extreme sensitivity of MW signals from clouds over complex topography and highly variable land surfaces found in mountainous regions (Habib *et al.*, 2012).

To exploit the advantages of using disparate sources of precipitation estimates from space for weather, climate and hydrological applications, a wide range of high-resolution precipitation products have been developed from the merging of data from spaceborne PR/MW/IR sensors. These products include TRMM's Multi-Satellite Precipitation Analysis (TMPA; Huffman *et al.*, 2007), the Climate Prediction Center (CPC) Morphing technique dataset (CMORPH; Joyce *et al.*, 2004), the Precipitation Estimation from Remote Sensing Information using an artificial neural network (PERSIANN; Hsu *et al.*, 1997), and the Global Satellite Mapping of Precipitation

(GSMaP; Kubota *et al.*, 2007). However, few validation studies of these products against rain gauge data collected in mountainous regions like the TP have been performed due to the difficulty in obtaining warm precipitation retrievals from spaceborne MW radiometers and the sparse distribution of rain gauges in such regions. For example, GSMaP-derived rainfall amounts and detection rates become less accurate with increasing altitude over the Nepalese portion of the Himalayas (Shrestha *et al.*, 2012). Precipitation peak times from TMPA, CMORPH, PERSIANN, and GSMaP datasets either lag behind or are ahead of rain gauge-observed precipitation peak times by several hours over south-facing slopes of the Himalayas (Yamamoto *et al.*, 2011).

As an important source of complementary data to satellite retrievals, rain gauge data can reveal the diurnal cycle of precipitation at a high temporal resolution (Dai, 2001; Li *et al.*, 2008), as well as identify the source of precipitation processes. For instance, the warm-season rainfall to the east of the TP has been found to originate over the highlands in the mid-afternoon hours and then propagate eastward or southeastward to adjacent lowlands at night or in the early morning (Yu *et al.*, 2007a, 2007b; Huang *et al.*, 2010). But this finding is limited to transition regions between the TP and its nearby plain. Studies about the diurnal variation in precipitation using *in situ* precipitation data are still not available over the main part of the TP. Moreover, the accuracy of the diurnal variation in precipitation relies on the density of rain gauge sites (Huffman *et al.*, 2007; Xie *et al.*, 2007). The topography of the TP has also been proven to strongly affect diurnal variations in precipitation and convective clouds, as observed from satellite data (Fujinami *et al.*, 2005). The satellite precipitation product merged with rain gauge measurements (e.g. the TRMM 3B42 product) has characterized the topographic effect of the diurnal variation of precipitation over the TP better than other products (Yamamoto *et al.*, 2011). Given the dual influences of complex topography and highly variable land surfaces, diurnal variations in warm-season precipitation over the TP deserve further in-depth analyses using high-resolution satellite precipitation products, combined with *in situ* measurements from a high-density network of rain gauge sites. Such a network has recently been established and consists of 129 stations spread over the TP, except for parts of the northwestern region. The investigation of the diurnal cycle of precipitation from this high-density gauge-based network may provide important guidance for the development of rainfall retrieval algorithms from satellite and model verifications over the TP.

The objectives of this study are to (1) describe the spatial pattern of the diurnal cycle of rainfall over the TP, including not only frequency but also amounts with respect to both short- and long durations of rainfall, (2) identify regional characteristics of the diurnal variation in precipitation in relation to topography, and (3) perform a preliminary validation of the CMORPH product against rain gauge measurements and, in turn, explain any differences found in their respective rainfall diurnal

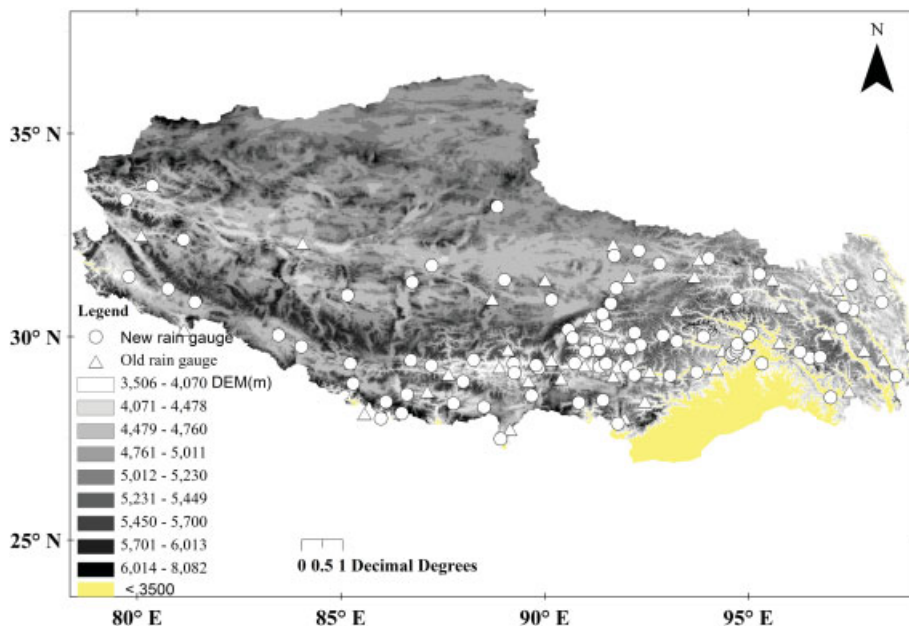


Figure 1. Spatial distribution of 39 rain gauge stations (white triangles) established prior to 2010 and 86 rain gauge stations (white circles) established in 2010 across the Tibetan Plateau. A GTOPO30 digital elevation model at 30-arc second resolution is superimposed on the map.

Table 1. Number of weather stations on the Tibetan Plateau at different altitudes.

Altitude (km)	<2.75	2.75–3	3–3.25	3.25–3.5	3.5–3.75	3.75–4	4–4.25	4.25–4.5	4.5–4.75	>4.75
N	9	5	8	6	17	25	14	18	18	5

Table 2. Information about the 12 rain gauge-equipped stations selected to study the diurnal cycle of precipitation over terrain types typical of the Tibetan Plateau.

Station	ID #	Lat (°N)	Lon (°E)	Altitude (m)	Terrain type
Bomi	0	29.87	95.77	2736	Valley
Changdu	1	31.15	97.17	3315	Valley
Zedang	2	29.25	91.77	3551	Valley
Lhasa	3	29.67	91.13	3648	Valley
Nielamu	4	28.18	85.97	3810	Valley
Rikaze	5	29.25	88.88	3836	Valley
Shiquanhe	6	32.5	80.08	4278	Highland
Dingri	7	28.63	87.08	4300	Highland
Naqu	8	31.48	92.07	4507	Highland
Namucuo	9	30.91	90.17	4751	Lake
Milashankou	10	29.8	92.35	4841	Mountain ridge
Mt. Everest	11	28.12	86.49	5032	Mountain ridge

cycles during the summertime over the TP. Data collected during the summer of 2010 and 2011 are used.

Section 2 provides a description of datasets and the methodology used in the study. Characteristics of the diurnal variation in precipitation fields from both CMORPH and the rain gauge network are examined in Section 3. Section 4 discusses possible mechanisms explaining the diurnal variation in precipitation using reanalysis data. Finally, conclusions are drawn in Section 5.

## 2. Data and methods

### 2.1. Study area

The premise of this study is that the TP, with its complex topography and high elevation, often experiences frequent precipitation events and exhibits a strong diurnal variation in precipitation during the summer when particular large-scale atmospheric conditions occur (e.g. the Asian summer monsoon). The Tibet Autonomous Region (Tibet for short) covers an area of over 1.2 million km<sup>2</sup>, taking up about three-quarters of the TP. Most parts of Tibet receive limited amounts of rainfall because they lie in the rain shadow of the Himalayas (Ramstein *et al.*, 1997; Xie *et al.*, 2006). The 129 weather stations established by the China Meteorological Administration (CMA) are geographically distributed across Tibet (Figure 1); site elevations range from 952 m to 5032 m. All weather stations include rain gauges and autonomous data-logging systems. Roughly 74% of the weather stations in Tibet are located at elevations ranging from 3.5 to 4.75 km ASL (Table 1). To our knowledge, this is the densest network of weather stations covering a wide range of altitudes and orographic settings over the central part of the TP. To assess the effects of altitude and topography (e.g. valleys or mountain ridges) on diurnal variations in precipitation, 12 stations representing different terrain types (Table 2), marked by white circles in Figure 2, have been selected for further analyses.

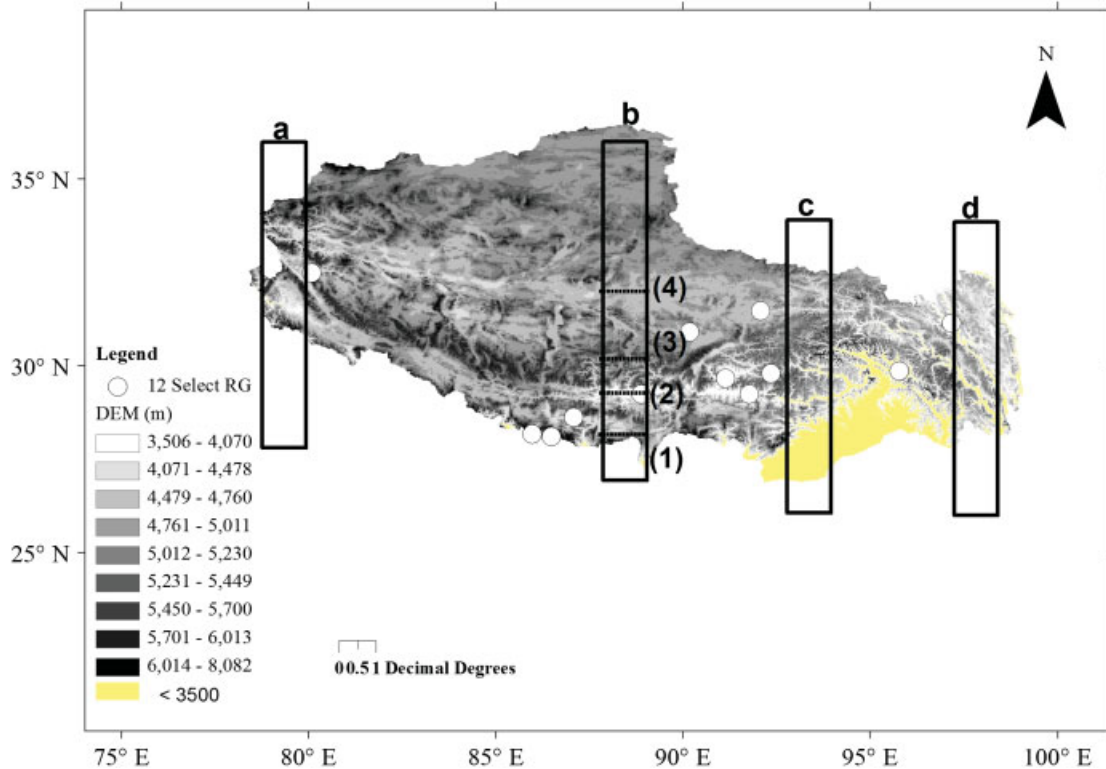


Figure 2. Locations of areas selected to study the meridional diurnal variation in precipitation over the Tibetan Plateau (rectangles a, b, c, and d). Rectangle b is further subdivided into four subregions: the Himalayan Mountain Range (1), the Yarlung TsangPo River Valley (2), the Nianqing Tanggulashan Mountain (3), and the North Tibet grassland (4). A GTOPO30 digital elevation model at 30-arc second resolution is superimposed on the map. The 12 rain gauge stations located on different terrain types typical of the Tibetan Plateau are denoted by white dots.

## 2.2. Rain gauge data

The Tibet Meteorological Services collect precipitation measurements at the 129 weather stations on an hourly basis. Data from the summer seasons of 2010 and 2011 are used in this study because these years contain full records of measurements from both newly established and existing stations. The summer season is defined as the months of June, July, August, and September. All data from each site are subject to the following quality checks. Temporal homogeneity tests described by Ding *et al.* (2008) and Feng *et al.* (2004) are first performed. A further requirement is that out of the total number of days of measurements over the two summer seasons at a site, more than 90% of the days must contain a complete set of measurements. Out of 129 rain gauge stations, 125 stations passed these quality control checks, so data from these sites are used in this study.

## 2.3. CMORPH precipitation data

The satellite precipitation data under consideration in this study is CMORPH (Joyce *et al.*, 2004), which incorporates precipitation estimates derived from four types of MW sensors onboard Sun-synchronous low earth-orbiting satellites. These sensors include the TRMM MW imager, the Advanced Microwave Sounding Unit, the Special Sensor Microwave Imager, and the Advanced Microwave Scanning Radiometer.

IR data onboard five geosynchronous meteorological satellites are used to infer the cloud motion vectors derived from spatial lag correlations of successive geostationary satellite IR images during time periods when MW data are not available. Owing to the limited coverage of MW images, time and space gaps of MW-based precipitation characteristics inevitably exist during the time period between the two successive MW overpasses. The flexible ‘morphing’ technique, a combination of various existing MW rainfall algorithms (Joyce *et al.*, 2004), is then applied to modify the shape and intensity of rainfall patterns. In particular, the vectors are used to propagate MW-based precipitation features through the time gap between the two successive MW overpasses. The shape and intensity of rainfall patterns in the intervening time periods between MW scans are then morphed using time-weighting linear interpolation. The weights are determined from forward (backward) advection, from the previous (the most current) to the most current (the previous) MW ‘snapshot’ of precipitation features.

The CMORPH precipitation product has been widely validated (e.g. Xie *et al.*, 2007; Dinku *et al.*, 2008; Sohn *et al.*, 2009; Kidd *et al.*, 2011; Stampoulis *et al.*, 2013), suggesting that it has great potential in identifying large-scale patterns and diurnal cycles of precipitation, among other applications. Given the topographically complex terrain characterizing the TP, satellite precipitation data with very high spatial resolution is especially needed. Of

the several merged satellite precipitation products (i.e. TMPA, PERSIANN, and GSMaP), the CMORPH product has the highest resolution (8 km) and so it is the most suitable product to use in studying precipitation patterns over the TP.

For a detailed description of the CMORPH algorithm, the readers are directed to refer Joyce *et al.* (2004). The version 1.0 CMORPH product, available starting from January 1998 at various spatial and temporal resolutions for regions between 60°N and 60°S, was used in this study. Gridded CMORPH data over the TP at an 8-km spatial resolution and a 30-minute temporal resolution was deemed adequate for the purposes of this study in terms of plateau- and local-scale analyses.

#### 2.4. Reanalysis data

The diurnal variation of precipitation in the extra-tropics is closely related to synoptic conditions. In order to discover a possible link between meteorological conditions and precipitation features, the European Centre for Medium-Range Weather Forecasts (ECMWF) and Re-Analysis Interim reanalysis data (ERA-Interim) (Uppala *et al.*, 2008) are used to examine seasonal averages and diurnal variations in both plateau- and local-scale circulation. The ERA-Interim dataset has 37 vertical levels ranging from 1000 hPa to 1 hPa, with a horizontal spatial resolution of 0.75° × 0.75° and a 6-hourly temporal resolution.

#### 2.5. Methodology

All measurements are recorded in Beijing time (*BJT*). To consider the effect of solar radiation on the diurnal variation in precipitation, the time coordinate was converted to local solar time (*LST*) using the equation

$$LST = BJT - 8 + Lon/15 \quad (1)$$

where Lon refers to the longitude of a given station. Each daily 24-hour period is divided into eight 3-hourly intervals and defined as follows (Singh and Nakamura, 2009): late night (00:00 hours–03:00 hours LST), early morning (03:00 hours–06:00 hours LST), morning (06:00 hours–09:00 hours LST), late morning (09:00 hours–12:00 hours LST), early afternoon (12:00 hours–15:00 hours LST), late afternoon (15:00 hours–18:00 hours LST), evening (18:00 hours–21:00 hours LST), and night (21:00 hours–24:00 hours LST).

In a complex orographic environment like this study area, differences in elevation over short distances can lead to significant changes in the distribution of precipitation due to the interaction between topography and the atmospheric flow. So a separate analysis of the diurnal cycle has to be performed at each station. Although Wallace (1975) demonstrated that harmonic analysis is a good method to use for examining the diurnal variation in precipitation, the simple harmonic pattern can differ greatly from the diurnal precipitation curve (Dai *et al.*, 1999). Direct examination of the hourly data collected during a day is made instead to determine the

maximum amount of precipitation and the preferred time of occurrence, i.e. the mean solar local time at which the maximum in precipitation amount occurs.

The diurnal cycle of rainfall amount and frequency are examined on the basis of the daily average distribution of hourly time series for the consecutive summertime seasons during 2010–2011. According to Sorooshian *et al.* (2002), the mean precipitation at a particular hour of the day,  $\bar{R}(x, y, t)$ , is expressed as

$$\bar{R}(x, y, t) = \sum_{d=1}^{d=\text{day}} R(x, y, t, d) / \text{day} \quad (2)$$

where  $R(x, y, t, d)$  is the precipitation amount at ‘*t*’ o’clock ( $t = 1, 2, \dots, 24$ ) on day number ‘*d*’ at a given station with coordinates (*x*, *y*), and ‘day’ is the total number of days during the two summertime periods when precipitation was observed. When the total precipitation amount accumulated in an hour is greater than or equal to 0.1 mm, this hour is called a precipitation hour. The average hourly precipitation was examined to identify the maximum in precipitation amount (amplitude) and the preferred time of occurrence (phase) during a particular day. The amplitude was then normalized, i.e. the maximum minus the 24-hour mean (Wallace, 1975; Dai *et al.*, 1999; Yu *et al.*, 2007a). The normalized amplitude is given in units of percent, which provides a measure of the magnitude of the diurnal cycle with respect to the 24-hour mean precipitation amount. For example, a normalized amplitude of 50% means that the magnitude of the maximum amount of precipitation is 1.5 times the 24-hour mean. The frequency of rain on a given day is calculated by noting if precipitation was recorded at ‘*t*’ o’clock. If the precipitation amount at ‘*t*’ o’clock and station (*x*, *y*) is more than 0.1 mm,  $R(x, y, t, d) = 1$ ; otherwise, it is equal to 0. In this way, time series of hourly precipitation amount and frequency during any time period can be obtained for each station.

Precipitation events were further classified according to duration, which is defined as the number of hours between the beginning and the end of one rainfall event. Methods described by Yu *et al.* (2007a) were used to discriminate precipitation types and their corresponding diurnal cycles. The intensity of rainfall during a short (e.g. convective rainfall) or long (e.g. stratiform rainfall) rainfall event can vary. A short (long) duration rainfall event that may be intermittent is defined here as rain falling for 1–2 hours (more than 3 hours) with no more than a total of 1 hour of no rain falling within the event. If the non-raining period lasts 2 hours and subsequently, rain begins again, this is classified as a new rainfall event.

### 3. Results

#### 3.1. Large-scale seasonal variations in precipitation and the wind fields

Seasonal mean synoptic states and how the rain band and wind circulation progresses from spring to winter over the

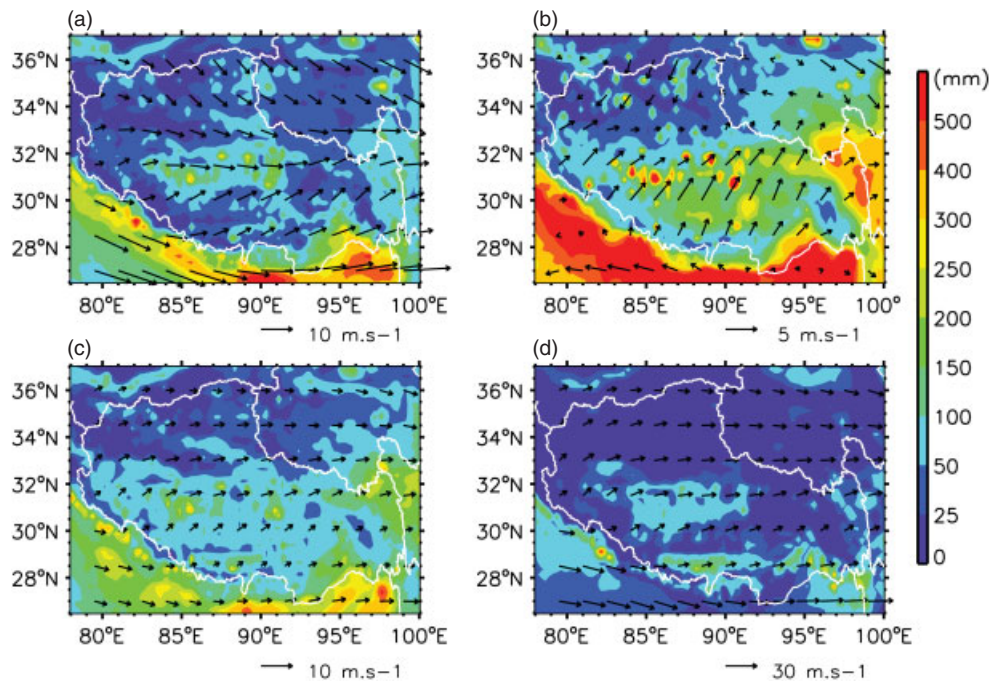


Figure 3. Average precipitation amount (filled contours) over the Tibetan Plateau derived from CMORPH data from 2001 to 2011, overlaid with the coincident large-scale wind field (arrows) at 500 hPa from ERA-Interim reanalysis for (a) spring, (b) summer, (c) autumn, and (d) winter.

TP are investigated. Figure 3 shows spatial patterns of mean precipitation amounts and wind vectors at 500 hPa during the four seasons. Over areas north of 32°N, winds change from north-westerlies (spring) to north-easterlies (summer), and then to westerlies in autumn and winter. Strong westerlies prevail in the lower troposphere across the whole plateau in winter.

In general, precipitation amounts increase steadily from spring to summer, then decrease during the autumn season and finally fizzle out in winter. In summer, the steering wind is south-westerly over most parts of the TP. South-westerlies and north-easterlies converge along 33°N, leading to more atmospheric instability which causes sporadic rainfall events. High-level prevailing south-westerlies (not shown in Figure 3) transport a large amount of water vapour from the Indian Ocean and the Bay of Bengal into the central-eastern part of the TP, resulting in a greater amount of precipitation in this region during the summer than in other seasons.

### 3.2. Diurnal variation in synoptic conditions

Divergence and relative humidity (RH) fields at 500 hPa and 200 hPa from ERA-Interim reanalysis data are examined to determine synoptic conditions affecting the occurrence and diurnal variation in summer precipitation over the TP. In this high-altitude region, the 500 hPa level roughly represents the surface level.

In the high troposphere over the TP (200 hPa), divergence dominates over almost all of the TP, except for peripheral regions; the highest RH is located in the south and decreases towards the north (Figure 4(a)). The differential divergence field at 200 hPa (Figure 4(b)) shows

stronger divergence in the late afternoon (18:00 hours LST) relative to the daily mean in the central part of the TP, while the reverse is seen along the southeastern edge. At the 500-hPa level, convergence dominates (Figure 4(c)), except along southern and northern edges of the plateau. In the central plateau, a stronger convergence prevails at 12:00 hours LST, relative to the daily mean (Figure 4(d)); divergence dominates over the southern and northern edges. By and large, lower-level convergence and upper-level divergence, along with the higher RH in the lower atmosphere, favour summer convection and precipitation production over the TP.

As shown in Figure 5, convergence at the 500 hPa level increases from early morning to late afternoon in the central part of the TP, then decreases towards midnight, when the moisture level is at its highest. Divergence in the upper atmosphere (Figure 6) varies diurnally in the same way as convergence, both of which have maxima over the central part of the TP during late afternoon into early evening. Over the northern part of the TP, morning peaks in precipitation are more likely seen (Figures 5(b) and 6(b)). In general, this examination of the diurnal cycle of synoptic conditions at two different atmospheric levels reveals that the time of day when precipitation events tend to occur over most of the TP is late afternoon to early evening.

### 3.3. Diurnal cycle of gauge-measured total precipitation

The spatial distribution of the time when the maximum precipitation occurs is used to discern spatial features of the diurnal peak phase. Vector plots represented by an

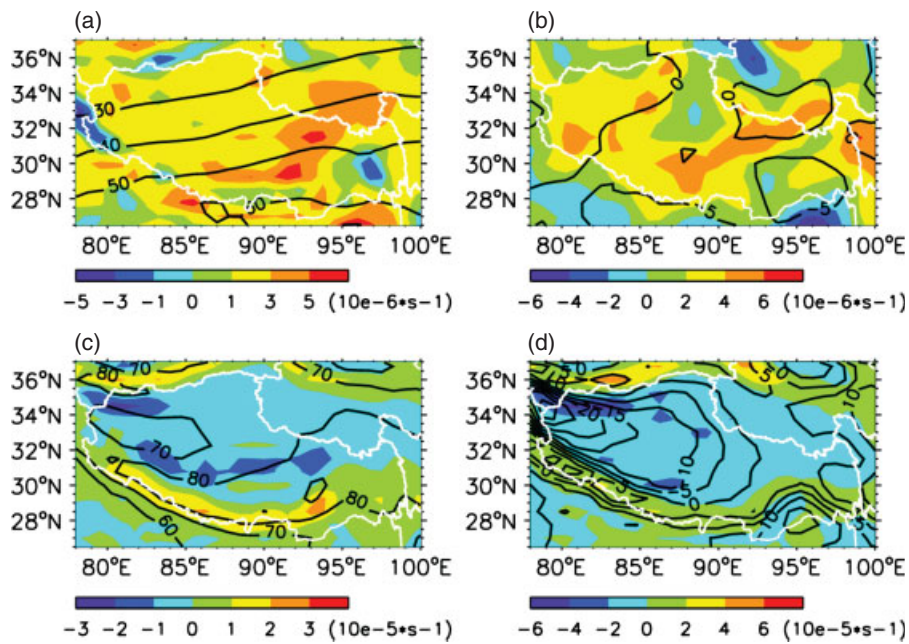


Figure 4. Daily mean RH (black contours, in %) superimposed on the divergence field (filled contours) at (a) 200 hPa (in units of  $10^{-6} \text{ s}^{-1}$ ) and (c) 500 hPa (in units of  $10^{-5} \text{ s}^{-1}$ ). Daily mean differences in RH (black contours, in %) superimposed on the differential divergence field (filled contours) at (b) 200 hPa (in units of  $10^{-6} \text{ s}^{-1}$ ), and (d) 500 hPa (in units of  $10^{-5} \text{ s}^{-1}$ ). Daily differences are calculated as the 12:00 hours UTC value minus the daily mean value. Negative values indicate convergence. The Tibetan Plateau is outlined in white.

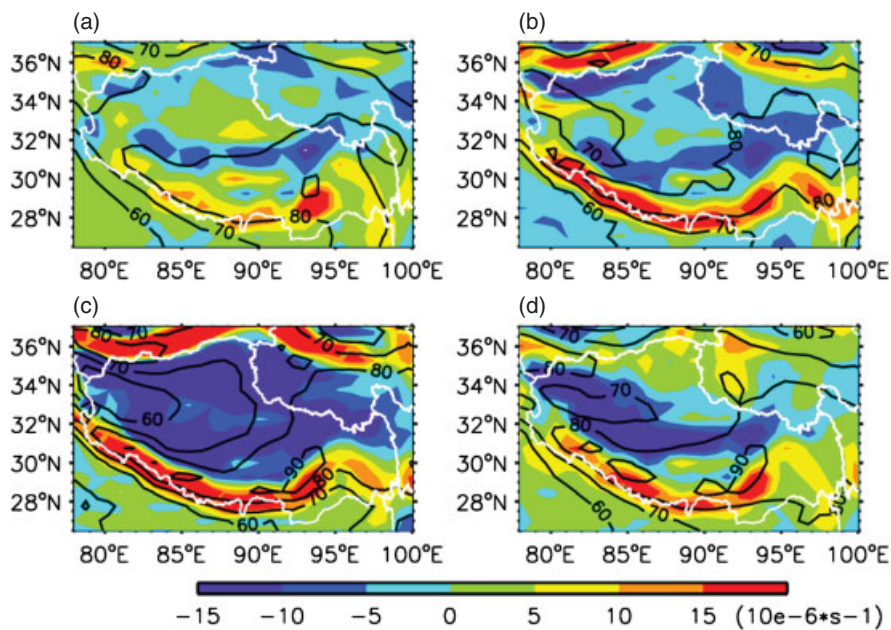


Figure 5. Average RH at 500 hPa (black contours, in %) superimposed on the divergence field (filled contours, in units of  $10^{-6} \text{ s}^{-1}$ ) at (a) 00:00 hours UTC (06:00 hours LST), (b) 06:00 hours UTC (12:00 hours LST), (c) 12:00 hours UTC (18:00 hours LST), and (d) 18:00 hours UTC (00:00 hours LST). Negative values indicate convergence. The Tibetan Plateau is outlined in white.

arrow pointer on a circular 24-hour clock dial are used to display the prevailing time (phase) of the maximum precipitation amount or frequency (Higgins *et al.*, 1996; Dai *et al.*, 1999; Yu *et al.*, 2007a). Figure 7(a) and (b) shows spatial distributions of the maximum hourly rainfall amount (frequency) and its corresponding phase at sites in Tibet during the summer seasons of 2010 and

2011. The arrow direction represents the phase at a given station and the length of the arrow represents precipitation amount (Figure 7(a)) or frequency (Figure 7(b)). Overall, about 60% of the 125 stations experience the greatest precipitation amounts and number of precipitation events in the afternoon-to-evening period. In western Tibet, both maximum precipitation amount and frequency are

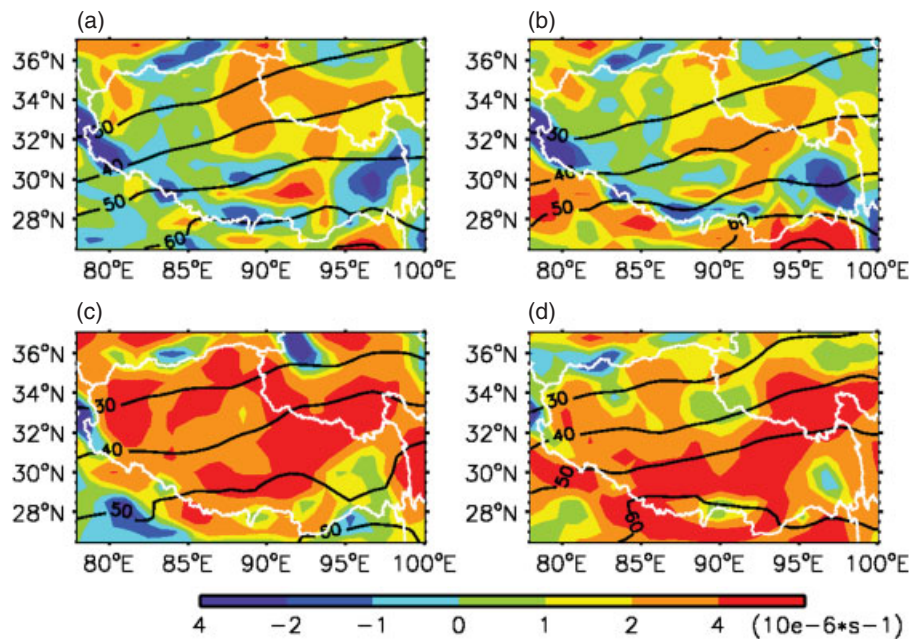


Figure 6. Average RH at 200 hPa (black contours, in %) superimposed on the divergence field (filled contours, in units of  $10^{-6} \text{ s}^{-1}$ ) at (a) 00:00 hours UTC (06:00 hours LST), (b) 06:00 hours UTC (12:00 hours LST), (c) 12:00 hours UTC (18:00 hours LST), and (d) 18:00 hours UTC (00:00 hours LST). Negative values indicate convergence. The Tibetan Plateau is outlined in white.

relatively smaller in magnitude, presumably because the water vapour content over that area is lower (Figure 4(a)).

The non-uniform spatial distribution of the timing of the maximum frequency and amount of precipitation shown in Figure 7 is similar to that found in India, which is located immediately to the south of the TP (Deshpande and Goswami, 2013). This figure suggests that a single mechanism alone cannot account for the complicated nature of diurnal variations in precipitation over the TP. It is to be noticed that no prevailing nocturnal maximum in precipitation can be identified across Tibet, either in terms of amount or in terms of frequency. Geographically speaking, the afternoon-to-evening peak in precipitation dominates at stations located in the Yarlung TsangPo Valley of the central TP. Along the north slope of the Himalayas, a morning peak is observed while on the south slope of the Himalayas, nocturnal precipitation dominates (Yamamoto *et al.*, 2011). The latter may be caused by the huge shielding effect of the Himalayas and the Karakoram Mountain range (Lin and Wu, 1990; Avey *et al.*, 2007).

A cluster in the diurnal phase distribution of precipitation frequency can be found in the region south of  $31^{\circ}\text{N}$ . Maxima in frequency are seen in the late morning or early afternoon at stations located near mountain ridges, and in either late afternoon or evening for those stations located in valleys. Although some general patterns in the diurnal cycle of precipitation amount are seen, the cycle over the TP is still complicated. For example, in the southeastern part of the TP where the elevation is relatively lower, neighbouring stations can experience both daytime and nocturnal maxima in precipitation amount.

### 3.4. Diurnal cycle of gauge-measured short- and long-duration precipitation events

The diurnal variation in precipitation with respect to the duration of precipitation events is examined in this section. A short-duration rainfall event is defined as one lasting from 1 to 2 hours and a long-duration rainfall event is defined as the one lasting for more than 3 hours. Figure 8 shows the distribution of percentages of rainfall amount and frequency associated with short- and long-duration precipitation events and Figure 9 summarizes the timing of maximum hourly rainfall amount and frequency associated with short- and long-duration precipitation events at all stations in the TP. As revealed in Figure 8(c) and (d), short-duration precipitation events are more frequent than long-duration precipitation events (by about 10–30%). More than 70% of total rainfall amounts accumulate during long-duration rainfall events over the TP (Figure 8(b)), which mainly occur during the late morning to the afternoon (Figure 9(b)). The afternoon peak can be attributed to convective precipitation caused by the solar heating effect, which is corroborated by the diurnal cycle of the large-scale circulation generated from reanalysis data (Figures 5 and 6). Note that the late morning maxima in precipitation seen in rain gauge data and also in radar measurements collected during a field campaign carried out in the central part of the TP (Hirose and Nakamura, 2005) are missing in the reanalysis dataset. The presence of a late-morning maxima in precipitation is attributed to a persistent mesoscale system located in this region, which more often than not produces long-duration precipitation events during that time of the day. An interesting feature is that there is no coherent spatial

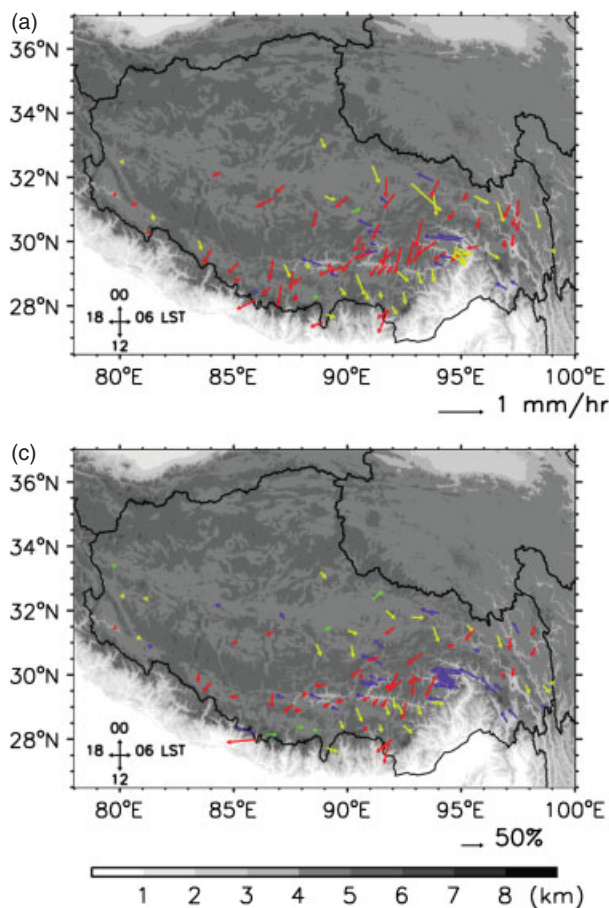


Figure 7. Diurnal phase and amplitude of rainfall averaged over the summer months of 2010 and 2011 according to (a) maximum hourly rainfall amount and (b) maximum hourly rainfall frequency. The direction towards which an arrow points denotes the local solar time (LST) when the maximum occurs (shown on the clock dial in the lower left corner of each plot) and the arrow length represents magnitudes of rainfall amount or frequency. The arrow direction denotes when the diurnal phases of a certain rain gauge occur: quadrant one (00:00–06:00 hours LST), quadrant two (06:00–12:00 hours LST), quadrant three (12:00–18:00 hours LST), and quadrant four (18:00–24:00 hours LST). Reference arrows represent 1 mm hour<sup>-1</sup> and 50% in panels (a) and (b), respectively. The grey shaded background shows the elevation.

pattern in rainfall amount from short-duration precipitation events (Figure 9(a)). Concerning rainfall frequency, Figure 9(c) shows that short-duration rainfall events tend to occur during the morning (03:00 hours–12:00 hours LST, corresponding to early morning, morning and late morning as defined in Section 2.5), whereas long-duration rainfall events have a coherent afternoon–evening–night diurnal cycle (12:00 hours–24:00 hours LST) except at some stations, where late morning maxima are evident (yellow arrows in Figure 9(d)).

Diurnal cycles associated with long-duration precipitation events have an overlap in the afternoon in terms of precipitation amount and frequency (Figure 9(b) and 9(d)). In addition, more than 70% of total rainfall amounts accumulate during long-duration rainfall events over the TP (Figure 8(b)). This suggests that oft-occurring (roughly 50% as shown in Figure 9(d)) long-duration

precipitation events in the afternoon are responsible for most of the rainfall amount for the whole day.

### 3.5. Diurnal cycle of CMORPH-based precipitation

The gauge-based diurnal cycle of precipitation demonstrates that the distribution of the diurnal phase over much of the TP is non-uniform, especially in the eastern and southernmost parts of the TP where the terrain is complex. Local-scale phenomena, such as ridge–valley effects, are expected to have their greatest impact on the distribution of the peak time of precipitation in places where large-scale dynamical processes are weak. To verify this, CMORPH precipitation data is used to investigate diurnal variations and their relation to topography over four regions from west to east over the TP (Figure 2). Prior to the analysis, a preliminary validation of CMORPH precipitation data against rain gauge data was performed. Regarding the diurnal phase of the precipitation amount, CMORPH-retrieved precipitation peaks generally lag 0–12 hours behind those seen in rain gauge data (Figure 10(a)). Figure 10(b) shows that CMORPH-derived total precipitation amounts are systematically overestimated, irrespective of station elevation. This overestimation of precipitation is probably due to contamination from signals that are scattered from all over the complex terrain.

Figure 11 shows the uniform nighttime and early morning local peaks in precipitation over the southern slope of the Himalayas from west to east, broadly consistent with previous findings (Yamamoto *et al.*, 2008; Singh and Nakamura, 2009; Deshpande and Goswami, 2013). This is possibly due to an increase in convection by the nighttime low-level convergence produced by katabatic mountain winds (Deshpande and Goswami, 2013). Proceeding northward from the foothills to the mountaintops of the Himalayas, the peak time of precipitation varies greatly from late night or early morning to late morning or afternoon.

Upon reaching the plateau area, large diurnal variations in precipitation are no longer seen in the meridional direction and precipitation mainly occurs in the late afternoon into evening, regardless of terrain. As will be shown in the following section, rain gauge data can better capture changes in the diurnal cycle of precipitation due to terrain.

### 3.6. Diurnal cycle over typical terrain: gauge versus CMORPH data

The terrain and land surface play significant roles in the diurnal cycle of precipitation due to the complexity of earth–atmosphere interactions. In order to characterize specific diurnal variations in precipitation from both rain gauge and CMORPH data over a given location on the TP, 12 stations with varying geographic characteristics were selected for a further detailed analysis (Table 2). Locations of these stations include mountain ridges and valleys, as well as a lake in central Tibet and highlands in northern Tibet.

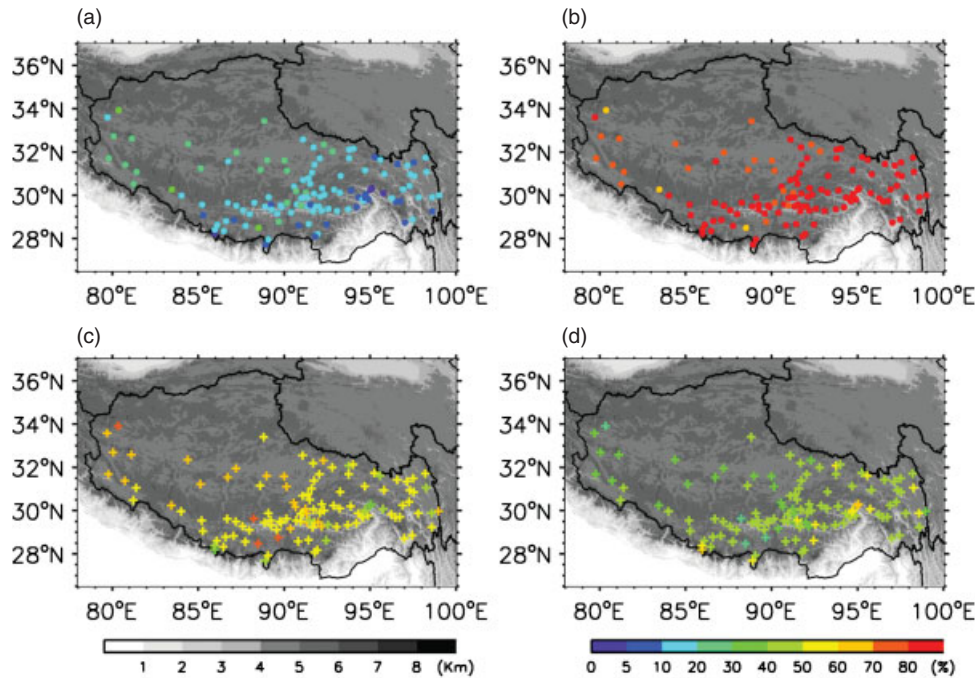


Figure 8. Distribution of rainfall amount percentages (represented by solid circles) relative to total rainfall amounts for (a) short-duration rainfall events and (b) long-duration rainfall events and rainfall frequency percentages (represented by plus signs) relative to the total number of rainfall events for (c) short-duration rainfall events, and (d) long-duration rainfall events. Data are averaged over the period of June to September of 2010 and 2011. The grey shaded background shows the elevation.

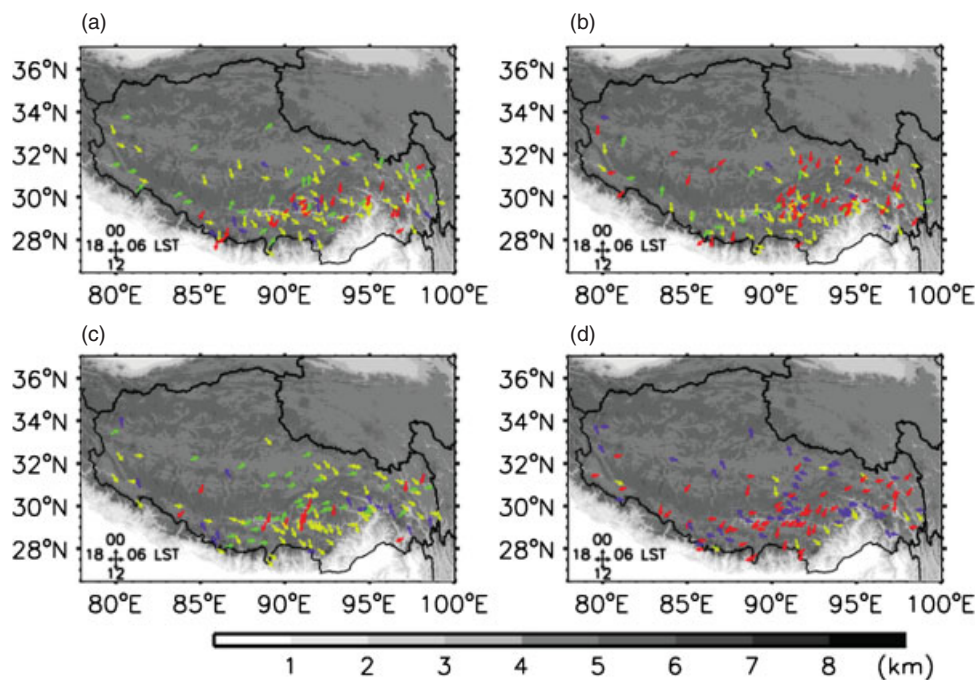


Figure 9. Distribution of the diurnal phase for short-duration rainfall events in terms of (a) maximum hourly rainfall amount and (c) maximum hourly rainfall frequency; and for long-duration rainfall events in terms of (b) maximum hourly rainfall amount, and (d) maximum hourly rainfall frequency. The direction towards which an arrow points denotes the local solar time (LST) when the maximum occurs (shown on the clock dial in the lower left corner of each plot). The arrow direction denotes when the diurnal phases of a certain rain gauge occur: quadrant one (00:00–06:00 hours LST), quadrant two (06:00–12:00 hours LST), quadrant three (12:00–18:00 hours LST), and quadrant four (18:00–24:00 hours LST). Data are averaged over the period of June through September of 2010 and 2011. The grey shaded background shows the elevation.

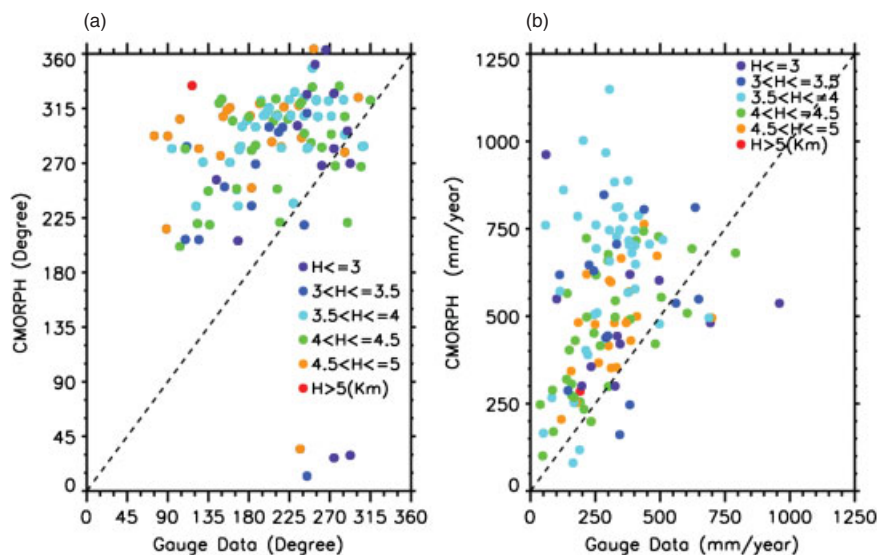


Figure 10. CMORPH-retrieved (a) diurnal phase (units in degrees ranging from  $0^{\circ}$  to  $360^{\circ}$ , corresponding to 0–24 hours), and (b) total rainfall amount (units in  $\text{mm year}^{-1}$ ) as a function of corresponding gauge-based measurements. The dashed line represents the 1:1 line and the shaded dots represent station altitudes.

Figures 12 and 13 show diurnal cycles of the normalized precipitation amount and precipitation frequency, respectively, based on rain gauge and CMORPH data. In general, the peak time of the CMORPH-retrieved maximum precipitation amount lags systematically behind that from rain gauge measurements by several hours (e.g. 9 hours at Namcuo). At Mt. Everest, peak timings of precipitation amount and frequency from CMORPH and rain gauge data are out of phase, suggesting that there are large uncertainties in the CMORPH precipitation product over regions covered by a perennial snowpack.

Rain gauge-based precipitation amounts and frequencies over the hilly region of the TP have generally larger values during the daytime. Sites located in valleys and by lakes show large late afternoon or evening peaks; a minor morning rainfall peak is seen at Namcuo. The amplitude of the diurnal variation near the lake site is lower than that at sites located in valleys and hilly regions. Compared to the latter sites, the mean precipitation amount at Namcuo is slightly higher and has a much weaker diurnal cycle because of the large body of water near this site. At the Shiquanhe station in the western part of the TP, a late-morning (09:00 hours–12:00 hours LST) secondary rainfall peak is observed.

Characteristics of the diurnal variation in precipitation vary with different land cover type. The following three pairs of neighbouring stations with different land surface types were chosen to explore possible differences in precipitation peak times between sites located close to one another: (1) Milashankou (ridge) and Lhasa (valley), (2) Mt. Everest (mountain top) and Dingri (valley), and (3) Naqu (highland) and Namcuo (large lake). There are distinct transitions in the peak time of gauge-based precipitation amounts from hilly regions down toward lakes or valleys, indicating that local circulation plays an important role in such a topographically complex

region as the TP. The finding of a phase transition agrees with previous results (Liu *et al.*, 2009; Singh and Nakamura, 2009). CMORPH data does not show such a phenomenon.

### 3.7. Zonal propagation of precipitation revealed from CMORPH data

The mean diurnal cycle of summertime precipitation over the TP is summarized in Figure 14, which shows a time-longitude diagram for the  $27^{\circ}\text{N}$ – $34^{\circ}\text{N}$  latitudinal band. Note that over almost all of the TP ( $82^{\circ}\text{E}$ – $99^{\circ}\text{E}$ ), more precipitation occurs during the time period of 15:00 hours to 21:00 hours LST. By contrast, the early morning or late night precipitation peak dominates over the westernmost part of the TP ( $79^{\circ}\text{E}$ – $82^{\circ}\text{E}$ ). Compared to the non-uniform pattern in precipitation phase shown in Figures 7 and 8, CMORPH data fails to capture local effects (for instance, the mountain ridge–valley effect) on diurnal variations in both precipitation amount and frequency.

The uniform diurnal peak time of late-afternoon-to-evening precipitation over the TP shows that there is no apparent propagation of this pattern in the west–east direction. This result stands out in stark contrast to the eastward propagation of precipitation from the eastern TP to the Sichuan Basin reported by Huang *et al.* (2010) and Yu *et al.* (2007a).

## 4. Discussion

### 4.1. Discrepancies between CMORPH and rain gauge data

Data from a dense network of rain gauge stations, together with CMORPH data, have been used to characterize the diurnal cycle of precipitation over the TP. Rain gauge data provide more detailed information at a local

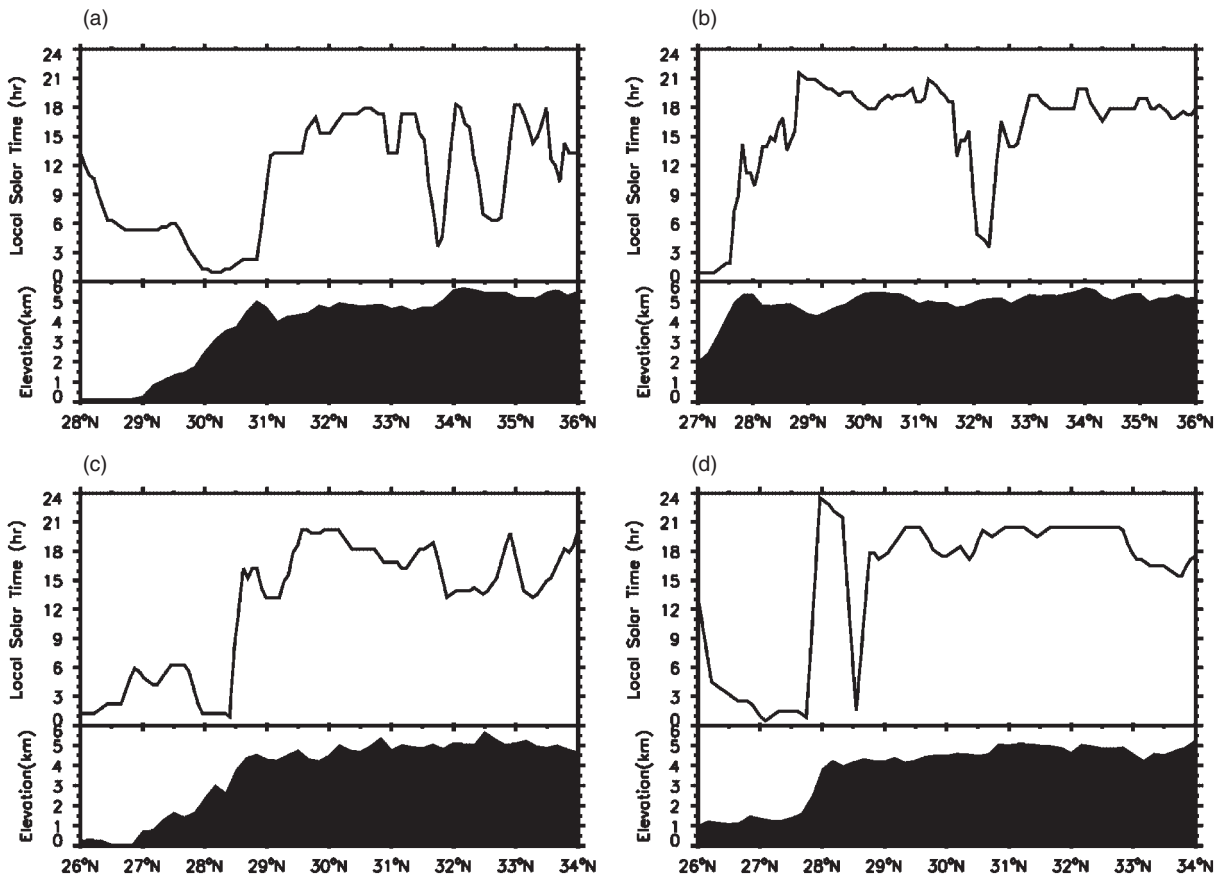


Figure 11. Meridional variation of the diurnal cycle of precipitation amount along four different strips (a, b, c, and d in Figure 2), superimposed on the corresponding terrain (black filled areas).

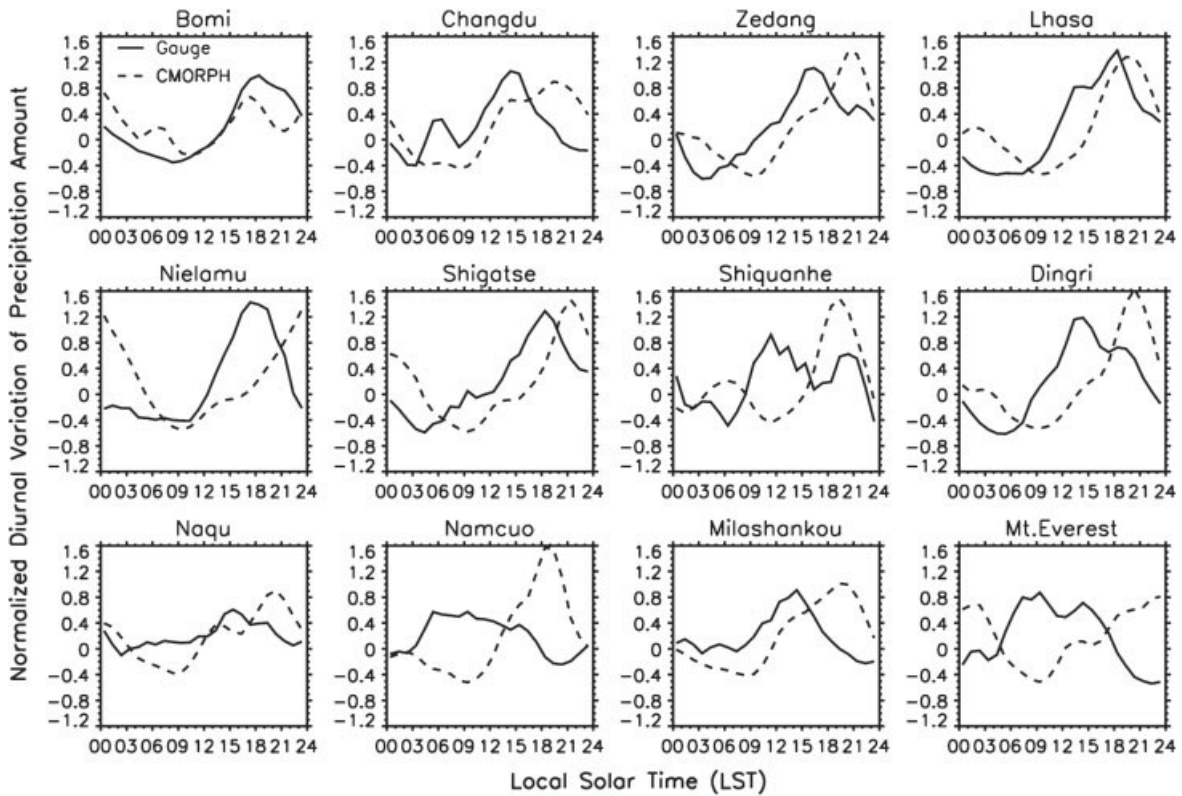


Figure 12. Normalized diurnal variation of precipitation amount in terms of gauge measurements (solid lines) and CMORPH data (dashed lines) at the 12 rain gauge stations shown in Figure 2. The amplitude is normalized by the 24-hour mean.

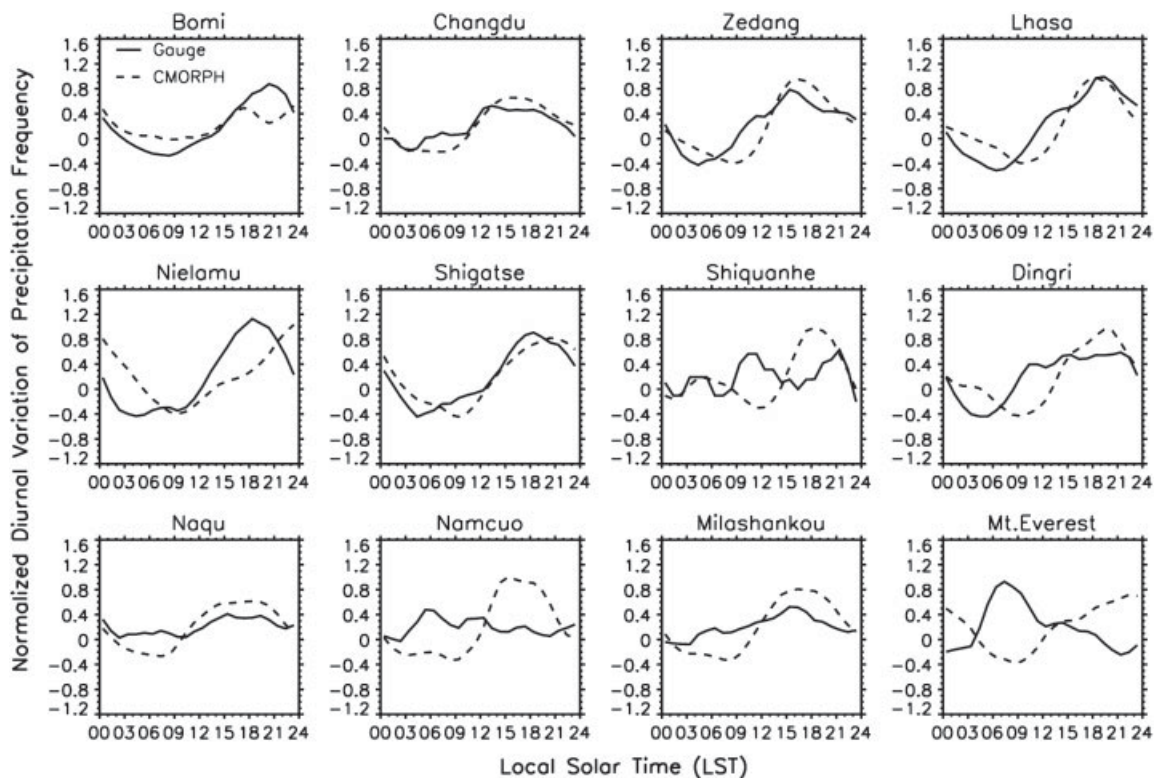


Figure 13. Meridional variation of the diurnal cycle of precipitation frequency along four different strips (a, b, c, and d in Figure 2), superimposed on the corresponding terrain (black filled areas).

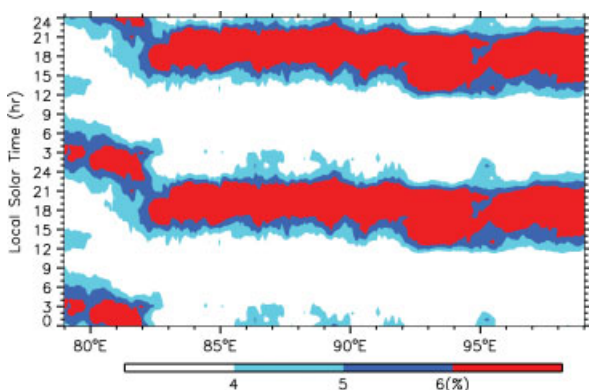


Figure 14. Time-longitude cross-section of the mean percentage of hourly precipitation during the period of June to September of 2010 and 2011 for the latitude band of 27°–34°N. The mean diurnal cycle was computed based on analyses of CMORPH data in 30-minute intervals (48 per day). In the absence of any diurnal cycle, the expected percentage is 4.2% for a 1-hour interval.

scale with regard to the diurnal variation of precipitation, especially at locations where the terrain is highly variable. CMORPH data can provide insight into the diurnal cycle over the TP on a plateau scale due to its wide spatial coverage. Certain discrepancies between the two datasets in capturing the diurnal cycle have been discovered and are discussed here.

In terms of both precipitation amount and its diurnal cycle, there are large uncertainties in the CMORPH

dataset, as illustrated in Figure 10. The half-hourly 8-km CMORPH dataset was resampled onto a 0.5°-latitude/longitude grid centred over each rain gauge site collecting data on an hourly basis. Mean values of the co-located spatial and temporal ensemble were then used in the regression analysis. Uncertainties will inevitably be introduced during the process of point-to-pixel collocation of precipitation data over the TP.

MW signals (the precipitation proxy for CMORPH) scattered by clouds are sensitive to complex terrain (Habib *et al.*, 2012). Precipitation estimates from the CMORPH product are mainly retrieved from four types of MW sensors (Joyce *et al.*, 2004). The under-representation of hydrometeor variability within precipitating clouds and partial beam filling generally lead to inherent uncertainties in precipitation products from passive MW sensors like the TMI or TRMM (Harris *et al.*, 2003). On the other hand, the estimation method involving morphing cannot retrieve precipitation over snow- or ice-covered surfaces, which are found on some parts of the TP. These may be factors contributing to the discrepancy in diurnal cycles of precipitation derived from both satellite and rain gauge data over the TP.

Figure 14 shows that morning peaks in precipitation do not appear in the CMORPH dataset even though such peaks are occasionally seen in rain gauge data from sites located in the highlands (Figure 7). Except at a few mountain stations, peaks in rainfall amount from rain gauges are generally a few hours ahead of the peak time observed from CMORPH data. The same significant

discrepancy was also observed on the south-facing slope of the Himalayas by Yamamoto *et al.* (2011), suggesting that a further validation of satellite precipitation products should be done in mountainous areas like the TP. A detailed description of the validation of high-resolution CMORPH precipitation products against rain gauge data is in preparation by the authors.

#### 4.2. Possible mechanisms for the variability in diurnal cycles

The TRMM PR was reportedly able to detect both large- and small-scale precipitation systems over central Tibet (Hirose and Nakamura, 2005). The PR is expected to play a critical role in discriminating between convective and stratiform rainfall, which would deepen the understanding of possible mechanisms involved in explaining the diurnal variation in precipitation over the TP. However, ground-based radar measurements from

the first and second TP Experiment during the summers of 1979 and 1998 showed that more than 60% of rain events in most parts of the plateau, and in particular, more than 90% of rain events in the central plateau, such as along the Yarlung TsangPo Valley, were convective during the summertime (Qian *et al.*, 1984). These surface observations were in contradiction to retrievals from the TRMM PR, which showed that stratiform rainfall dominated during the summer (Fu and Liu, 2007). This discrepancy was attributed to the misidentification of the TRMM PR bright band due to the relatively high elevation of the TP land surface. This is why rainfall duration, rather than rainfall type, was considered in this study.

Figure 15 shows a latitude-pressure cross-section of RH and divergence fields averaged over 88°E–89°E. During the daytime, solar heating dominates over the TP. At 00:00 hours UTC (06:00 hours LST), there is

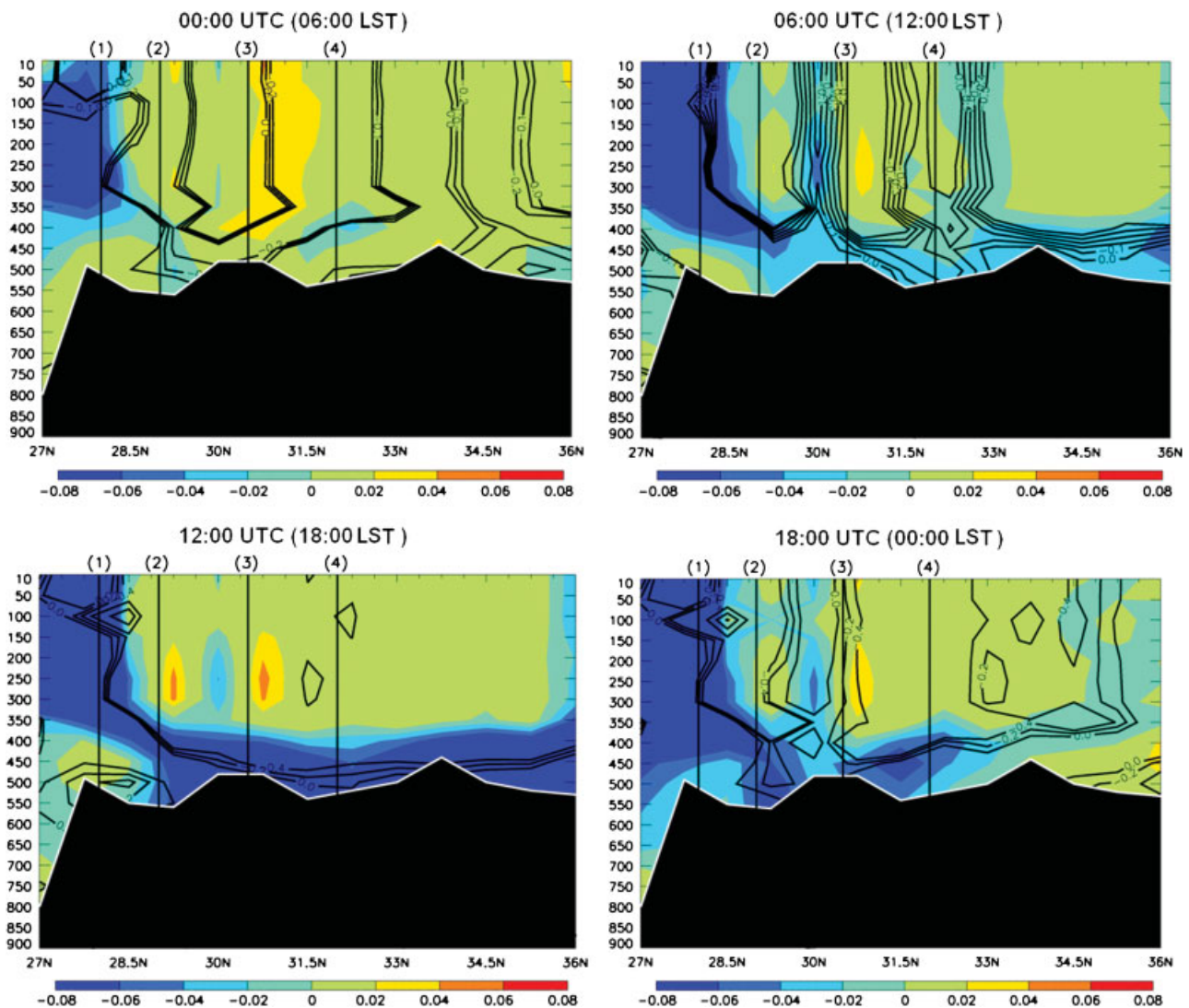


Figure 15. Pressure-latitude cross-sections of vertical wind velocity (black contour lines, in units of  $\text{m s}^{-1}$ ) and the divergence field (filled contours, in units of  $\times 10^{-5} \text{s}^{-1}$ ) at 00:00 hours UTC, 06:00 hours UTC, 12:00 hours UTC, and 18:00 hours UTC, which are averaged over 88°–89°E (strip b in Figure 2) during the period of June to September of 2010 and 2011. Black contours lines are plotted in  $0.1 \text{ m s}^{-1}$  intervals for panels (a) and (b) and in  $0.2 \text{ m s}^{-1}$  intervals for panels (c) and (d). ERA-Interim data is used here. Lines (1), (2), (3), and (4) shown in Figure 2 are drawn as well.

no distinct atmospheric motion in the vertical direction over the TP. From 06:00 hours UTC (12:00 hours LST) to 18:00 hours UTC (00:00 hours LST), a prominent upward motion is seen over the entirety of the TP. The upward motion increases and reaches a maximum at 12:00 hours UTC due to the stronger surface heating. During the time period of 12:00 hours UTC (18:00 hours LST) to 18:00 hours UTC (00:00 hours LST), the ascending motion over the TP decreases gradually and almost disappears by 06:00 hours UTC. The diurnal variation in vertical motion corresponds well with the time period when precipitation events tend to occur (15:00 hours–21:00 hours LST), as revealed by CMORPH data. Again, local mountain-valley flows, low-level nocturnal jets, and so on, which determine the predilection for precipitation events in the morning or late night as seen from rain gauge data, are not captured in the CMORPH dataset. The relatively coarse resolution of the ERA-Interim reanalysis ( $0.75^\circ$ ) is one of the main reasons why it cannot resolve local effects.

It has been historically recognized that both local weather and precipitation are readily influenced by orography (Riehl, 1954). So, local-scale topography (lake–land contrast and ridge–valley effects) could play an important role in rainfall distributions where large-scale dynamical processes are weak. A possible mechanism is that daytime heating and nighttime cooling over high terrain generates convergence over mountaintops during the day and divergence at night, respectively. Nighttime cooling over the higher terrain suppresses convection at the mountaintop. However, if the downslope motion resulting from radiative cooling at night converges with a low-level, moist, and unstable air current, then nocturnal precipitation may occur (Barros *et al.*, 2000, 2004; Kuwagata *et al.*, 2001; Lang and Barros, 2002). This effect is especially pronounced over the highest parts of the Himalayan range that are located at lower latitudes where solar insolation is direct (Houze, 2012).

Note that this analysis was conducted using data collected over the TP during only two warm seasons. Some apparent diurnal variations (e.g. the morning peak with respect to long-duration precipitation) may be due to strong mesoscale systems that produced precipitation not linked to any diurnally varying forcing mechanism. Further study focused on interactions between plateau-scale synoptic systems and regional mountain–valley circulation systems, and their impact on the specific diurnal cycle of precipitation at a given location on the TP, is required.

## 5. Conclusions

Diurnal cycles of mean precipitation amount and frequency over the TP have been investigated using two years (2010–2011) of summertime hourly precipitation data from a dense network of automatic weather stations and a high-resolution satellite precipitation product (CMORPH). Maxima in precipitation amount and

frequency from both datasets are associated with the afternoon-to-evening precipitation regime at approximately 60% of the stations comprising the rain gauge network. No west-to-east propagation of any diurnal variation in the timing of the maximum precipitation amount over the TP is seen.

The diurnal variation in the duration of rainfall events in the TP is also investigated. Short-duration rainfall events are more common than long-duration rainfall events (by about 10–30%), but the latter is responsible for the bulk of total precipitation amounts. More than 70% of total rainfall amounts come from long-duration rainfall events. Also, rain gauge measurements show that the diurnal variation in precipitation changes noticeably with respect to local topography. For instance, sites located in hilly regions tend to have a daytime peak in precipitation amount while those along lakes and in valleys have peaks in the evening into the nighttime. Rain events occur more frequently in the late morning or early afternoon at high-lying mountain stations and in the late afternoon or evening at sites located in valleys. In general, the diurnal variation in precipitation amount and frequency is similar, consistent with results from other studies.

A preliminary validation of CMORPH-retrieved precipitation amounts over the TP using rain gauge measurements as the ground truth has been performed. CMORPH retrievals overestimate precipitation amounts, while peak times of the maximum precipitation amount systematically lag behind those derived from rain gauge data. These discrepancies are partly due to high uncertainties inherent to MW sensors, which have difficulty in acquiring scattered signals over such a complex terrain as the TP.

Using ERA-Interim reanalysis data ( $0.75^\circ$  resolution), possible causes for the observed discrepancy between rain gauge-calculated and CMORPH-retrieved precipitation diurnal cycles from the perspective of large-scale circulation have been investigated. Local mountain–valley flows, low-level nocturnal jets, and so on, presumably reflecting the predilection for precipitation events in the morning or late night as seen from rain gauge data, are not captured by the CMORPH dataset. Its relatively coarse resolution is one of the main reasons why this dataset cannot resolve local effects. This suggests that satellite observations like CMORPH alone, even with its high temporal and spatial resolutions, cannot meet the requirement of determining the diurnal cycle of precipitation over the TP.

Therefore, a collective approach incorporating the individual merits of satellite retrievals, *in situ* ground-based measurements, and model estimations, while minimizing their limitations, should be undertaken. In particular, plateau-scale synoptic systems should be taken into account, combined with local circulation systems caused by the complex topography of the region. This would deepen, to some extent, our understanding of the diurnal cycle of precipitation over the TP.

## Acknowledgements

This study was financially supported by the Natural Science Foundation of China (grant no. 41171294/41175080), the Ministry of Science and Technology of the People's Republic of China (grant no. GYHY201206040/GYHY201306029, 2013CB955804), and the Chinese Academy of Meteorological Sciences (grant no. 2011Y002/2010Z002). We thank the anonymous referees for their thorough review and highly appreciate their comments that helped to improve the manuscript. Thanks also to the ECWMF website for providing online access to reanalysis data.

## 6. Conflict of interest

The authors have declared that there is no conflict of interest.

## References

- Avey L, Garrett TJ, Stohl A. 2007. Evaluation of the aerosol indirect effect using satellite, tracer transport model, and aircraft data from the International Consortium for Atmospheric Research on Transport and Transformation. *J. Geophys. Res. Atmos.* **112**: D10.
- Bai AJ, Liu CH, Liu XD. 2008. Diurnal variation of summer rainfall over the Tibetan Plateau and its neighboring regions revealed by TRMM multi-satellite precipitation analysis. *Chin. J. Geophys.* **51**(3): 518–528.
- Barros A, Joshi M, Putkonen J, Burbank D. 2000. A study of the 1999 monsoon rainfall in a mountainous region in central Nepal using TRMM products and rain gauge observations. *Geophys. Res. Lett.* **27**(22): 3683–3686.
- Barros AP, Kim G, Williams E, Nesbitt SW. 2004. Probing orographic controls in the Himalayas during the monsoon using satellite imagery. *Nat. Hazards Earth Syst. Sci.* **4**: 29–51.
- Carbone R, Tuttle J. 2008. Rainfall occurrence in the US warm season: the diurnal cycle. *J. Climate* **21**(16): 4132–4146.
- Dai A. 2001. Global precipitation and thunderstorm frequencies. Part II: diurnal variations. *J. Climate* **14**(6): 1112–1128.
- Dai A, Giorgi F, Trenberth KE. 1999. Observed and model-simulated diurnal cycles of precipitation over the contiguous United States. *J. Geophys. Res.* **104**(D6): 6377–6402.
- Deshpande NR, Goswami BN. 2013. Modulation of the diurnal cycle of rainfall over India by intraseasonal variations of Indian summer monsoon. *Int. J. Climatol.*, DOI: 10.1002/joc.3719.
- Ding Y. 1994. *Monsoons Over China*. Kluwer Academic Publishers: Dordrecht, The Netherlands.
- Ding Y, Wang Z, Sun Y. 2008. Inter-decadal variation of the summer precipitation in East China and its association with decreasing Asian summer monsoon. Part I: Observed evidences. *Int. J. Climatol.* **28**(9): 1139–1161.
- Dinku T, Chidzambwa S, Ceccato P, Connor S, Ropelewski C. 2008. Validation of high-resolution satellite rainfall products over complex terrain. *Int. J. Remote Sens.* **29**(14): 4097–4110.
- Feng S, Hu Q, Qian W. 2004. Quality control of daily meteorological data in China, 1951–2000: a new dataset. *Int. J. Climatol.* **24**(7): 853–870.
- Fu Y, Liu G. 2007. Possible misidentification of rain type by TRMM PR over Tibetan Plateau. *J. Appl. Meteorol. Climatol.* **46**(5): 667–672.
- Fujinami H, Nomura S, Yasunari T. 2005. Characteristics of diurnal variations in convection and precipitation over the southern Tibetan Plateau during summer. *Sola* **1**: 49–52.
- Habib E, ElSaadani M, Haile AT. 2012. Climatology-focused evaluation of CMORPH and TMPA satellite rainfall products over the Nile Basin. *J. Appl. Meteorol. Climatol.* **51**(12): 2105–2121.
- Harris D, Foufoula-Georgiou E, Kummerow C. 2003. Effects of underrepresented hydrometeor variability and partial beam filling on microwave brightness temperatures for rainfall retrieval. *J. Geophys. Res.* **108**(D8): 8380.
- Higgins RW, Janowiak JE, Yao YP. 1996. A gridded hourly precipitation database for the United States (1963–1993) in NCEP/Climate Prediction Center ATLAS No.1. U.S. Dep. of Comm., Washington, DC.
- Hirose M, Nakamura K. 2005. Spatial and diurnal variation of precipitation systems over Asia observed by the TRMM precipitation radar. *J. Geophys. Res. Atmos.* **110**: D5.
- Houze RA. 2012. Orographic effects on precipitation clouds. *Rev. Geophys.* **50**(1): Rg1001.
- Hsu K-L, Gao X, Sorooshian S, Gupta HV. 1997. Precipitation estimation from remotely sensed information using artificial neural networks. *J. Appl. Meteorol.* **36**(9): 1176–1190.
- Huang HL, Wang CC, Chen GTJ, Carbone RE. 2010. The role of diurnal solenoidal circulation on propagating rainfall episodes near the eastern Tibetan Plateau. *Mon. Weather Rev.* **138**(7): 2975–2989.
- Huffman GJ, Bolvin DT, Nelkin EJ, Wolff DB, Adler RF, Gu G, Hong Y, Bowman KP, Stocker EF. 2007. The TRMM multisatellite precipitation analysis (TMPA): Quasi-global, multiyear, combined-sensor precipitation estimates at fine scales. *J. Hydrometeorol.* **8**(1): 38–55.
- Joyce RJ, Janowiak JE, Arkin PA, Xie P. 2004. CMORPH: A method that produces global precipitation estimates from passive microwave and infrared data at high spatial and temporal resolution. *J. Hydrometeorol.* **5**(3): 487–503.
- Kidd C, Bauer P, Turk J, Huffman GJ, Joyce R, Hsu KL, Braithwaite D. 2011. Intercomparison of high-resolution precipitation products over northwest Europe. *J. Hydrometeorol.* **13**(1): 67–83.
- Krishnamurti T, Kishtawal C. 2000. A pronounced continental-scale diurnal mode of the Asian summer monsoon. *Mon. Weather Rev.* **128**(2): 462–473.
- Kubota T, Shige S, Hashizume H, Aonashi K, Takahashi N, Seto S, Takayabu Y, Ushio T, Nakagawa K, Iwanami K. 2007. Global precipitation map using satellite-borne microwave radiometers by the GSMaP Project: Production and validation. *IEEE Trans. Geosci. Remote Sens.* **45**(7): 2259–2275.
- Kuwagata T, Numaguti A, Endo N. 2001. Diurnal variation of water vapor over the central Tibetan Plateau during summer. *J. Meteorol. Soc. Jpn* **79**(1B): 401–418.
- Lang TJ, Barros AP. 2002. An investigation of the onsets of the 1999 and 2000 monsoons in central Nepal. *Mon. Weather Rev.* **130**(5): 1299–1316.
- Li J, Yu RC, Wang JJ. 2008. Diurnal variations of summer precipitation in Beijing. *Chin. Sci. Bull.* **53**(12): 1933–1936.
- Lin Z, Wu X. 1990. A preliminary analysis about the tracks of moisture transportation on the Qinghai-Xizang Plateau. *Geogr. Res.* **9**(3): 33–39.
- Liu LP, Feng JM, Chu RZ, Zhou YJ, Ueno K. 2002. The diurnal variation of precipitation in monsoon season in the Tibetan Plateau. *Adv. Atmos. Sci.* **19**(2): 365–378.
- Liu XD, Bai AJ, Liu CH. 2009. Diurnal variations of summertime precipitation over the Tibetan Plateau in relation to orographically-induced regional circulations. *Environ. Res. Lett.* **4**: 4.
- Qian Z, Zhang S, Shan F. 1984. *Analysis on Convective Activities Over the Tibetan Plateau in summer of 1979*. The Qinghai-Xizang Plateau Meteorological Experiment (1979) and Research Science Press: Beijing, China; 243–257.
- Ramstein G, Fluteau F, Besse J, Joussaume S. 1997. Effect of orogeny, plate motion and land-sea distribution on Eurasian climate change over the past 30 million years. *Nature* **386**(6627): 788–795.
- Riehl H. 1954. *Tropical meteorology*. McGraw-Hill: New York, NY.
- Shimizu S, Ueno K, Fujii H, Yamada H, Shirooka R, Liu LP. 2001. Mesoscale characteristics and structures of stratiform precipitation on the Tibetan Plateau. *J. Meteorol. Soc. Jpn* **79**(1B): 435–461.
- Shrestha M, Takara K, Kubota T, Bajracharya S. 2012. Verification of GSMaP rainfall estimates over the Central Himalayas. *J. Jpn. Soc. Civil Eng.* **67**(4): 37–42.
- Singh P, Nakamura K. 2009. Diurnal variation in summer precipitation over the central Tibetan Plateau. *J. Geophys. Res.* **114**(D20): D20107.
- Sohn BJ, Han H-J, Seo E-K. 2009. Validation of satellite-based high-resolution rainfall products over the Korean Peninsula using data from a dense rain gauge network. *J. Appl. Meteorol. Climatol.* **49**(4): 701–714.
- Sorooshian S, Gao X, Hsu K, Maddox R, Hong Y, Gupta H, Imam B. 2002. Diurnal variability of tropical rainfall retrieved from combined GOES and TRMM satellite information. *J. Climate* **15**(9): 983–1001.

- Stampoulis D, Anagnostou EN, Nikolopoulos E. 2013. *Assessment of high-resolution satellite-based rainfall estimates over the Mediterranean during heavy precipitation events*. *J. Hydrometeorol.* **14**(5): 1500–1514.
- Ueno K. 1998. Characteristics of plateau-scale precipitation in Tibet estimated by satellite data during 1993 monsoon season. *J. Meteorol. Soc. Jpn.* **76**(4): 533–548.
- Uppala S, Dee D, Kobayashi S, Berrisford P, Simmons A. 2008. Towards a climate data assimilation system: status update of ERA-Interim. *ECMWF Newsl.* **115**: 12–18.
- Wallace JM. 1975. Diurnal variations in precipitation and thunderstorm frequency over the conterminous United States. *Mon. Weather Rev.* **103**(5): 406–419.
- Wang CC, Chen GTJ, Carbone RE. 2005. Variability of warm-season cloud episodes over East Asia based on GMS infrared brightness temperature observations. *Mon. Weather Rev.* **133**(6): 1478–1500.
- Xie S, Xu H, Saji N, Wang Y, Liu WT. 2006. Role of narrow mountains in large-scale organization of Asian Monsoon Convection. *J. Climate* **19**(14): 3420–3429.
- Xie P, Chen M, Yang S, Yatagai A, Hayasaka T, Fukushima Y, Liu C. 2007. A gauge-based analysis of daily precipitation over East Asia. *J. Hydrometeorol.* **8**(3): 607–626.
- Yamamoto MK, Furuzawa FA, Higuchi A, Nakamura K. 2008. Comparison of diurnal variations in precipitation systems observed by TRMM PR, TMI, and VIRS. *J. Climate* **21**(16): 4011–4028.
- Yamamoto MK, Ueno K, Nakamura K. 2011. Comparison of Satellite precipitation products with rain gauge data for the khumb region, nepal himalayas. *J. Meteorol. Soc. Jpn.* **89**(6): 597–610.
- Yanai M, Li C, Song Z. 1992. Seasonal heating of the Tibetan Plateau and its effects on the evolution of the Asian summer monsoon. *J. Meteorol. Soc. Jpn.* **79**(1B): 419–434.
- Yanai M, Wu GX. 2006. *Effects of the Tibetan Plateau. Chapter 13, The Asian Monsoon*, Wang B (ed.), Springer: Chichester, UK; 513–549.
- Ye D, Gao Y. 1979. *The Meteorology of the Qinghai-Xizang (Tibet) Plateau*. Scientific Press: Beijing, China; 1–278.
- Yin ZY, Zhang X, Liu X, Colella M, Chen X. 2008. An assessment of the biases of satellite rainfall estimates over the Tibetan Plateau and correction methods based on topographic analysis. *J. Hydrometeorol.* **9**(3): 301–326.
- Yu R, Xu Y, Zhou T, Li J. 2007a. Relation between rainfall duration and diurnal variation in the warm season precipitation over central eastern China. *Geophys. Res. Lett.* **34**(13): L13703.
- Yu R, Zhou T, Xiong A, Zhu Y, Li J. 2007b. Diurnal variations of summer precipitation over contiguous China. *Geophys. Res. Lett.* **34**: L01704.